



Numerical investigation of electronic, dielectric and optical properties of CdO, SnO₂/CdO and SnO₂/CdO/PVP nanocomposites

A. Akouibaa¹ · R. Masrou² · A. Jabar² · G. Kadim² · M. Benhamou³ · A. Derouiche¹

Received: 2 March 2021 / Accepted: 11 September 2021 / Published online: 2 November 2021
© The Author(s), under exclusive licence to Springer Science+Business Media, LLC, part of Springer Nature 2021

Abstract

In this work, the electronic, optical and dielectric properties of pure CdO, mixed SnO₂/CdO and PVP coated SnO₂/CdO nanocomposites were calculated using the finite element method (FEM) and density functional theory. In this approach, the three studied nanostructures are modeled by the following geometric shapes: cubic-CdO, orthorhombic core/shell-SnO₂/CdO and nanorod SnO₂/CdO/PVP. The electronic structure shows that CdO and SnO₂/CdO have semiconductor character. The complex dielectric function, absorption spectra, refractive index, and reflectivity are discussed based on the electronic structure calculations. The obtained results using FEM confirm that the complex permittivity, absorption cross section, reflectivity and complex optical conductivity of CdO nanoparticle depend on their concentration in the surrounding medium and on the nature of the latter. The optical parameters spectra of CdO, SnO₂/CdO and CdO/SnO₂/PVP have the same evolution in the VU–Vis–NIR band. The effect of PVP coating on the optical properties of CdO/SnO₂/PVP nanocomposites is also studied.

Keywords Electronic properties · Optical properties · Nanocomposite · CdO–SnO₂–PVP · Finite element method

1 Introduction

Metal oxide nanostructures have immense attention of researcher in nanotechnology, because of their tremendous physical and chemical properties at nanoscale, which are very useful in various applications such as optoelectronics, sensor, catalyst, solar energy conversion, hydrogen generation and pollutant degradation (Fujishima and Honda 1972; Chen

✉ R. Masrou
rachidmasrou@hotmail.com

¹ LPPPC, Physics Department, Faculty of Sciences Ben M'sik, Hassan II University Casablanca, P.O. Box 7955, Casablanca, Morocco

² Laboratory of Solid Physics, Faculty of Sciences Dhar El Mahraz, Sidi Mohamed Ben Abdellah University, Atlas, BP 1796, Fez, Morocco

³ Dynamics of Complex Systems Team, Physics Department, Faculty of Sciences, Moulay Ismail University, P.O. Box 11201, Meknes, Morocco

et al. 2010; Subrahmanyam et al. 2014; Rakibuddin and Ananthkrishnan 2016; Lan et al. 2015). Consequently, numerous papers have been published over the last decade which includes the fundamental physical and chemical concepts, the technological optimization, the design and analysis of electronic devices. In particular transparent conducting oxide (TCO) materials possess unique combination of low resistivity and high optical transparency within the visible region of the electromagnetic spectrum. Cadmium oxide (CdO) is one of the promising representatives and the first to be used among these TCOs in solar cells since a long time (Jin et al. 2007). CdO semiconductor has intense interest due to their pure sodium chloride like crystal structure, high carrier mobilities ($142 \text{ cm}^2/\text{Vs}$), high electrical conductivities ($103 \text{ } \Omega^{-1} \text{ cm}^{-1}$) and a broad linear refractive index (Makori et al. 2014; Zhao et al. 2002; Karthik et al. 2018a, b), this makes CdO apply in various applications. Cadmium oxide is II-VI n-type semiconductor with a direct bandgap of 2.5 eV (Karthik et al. 2018a; Reddy et al. 2018). The band gap of CdO semiconductor nanomaterial is relatively small, which may show the way to the lower optical transparency in short wavelength region. Similarly, Tin oxide (SnO_2) based nanostructures have been one of the important oxide nanostructures owing to their important fascinating properties and various potential applications. It is a n-type with direct band gap 3.6 eV semiconductor material which possesses high electrical conductivity, extraordinary thermal and chemical stability, and high transparency (Anitha et al. 2016). Due to their key properties, SnO_2 has been used in various potential applications such as, catalytic applications, solar cells, semiconducting gas sensors, liquid crystal displays and protective coatings (Manjula et al. 2017). SnO_2 has been considered as an efficient photocatalyst due to its non-toxic nature, long-term stability and cost-effectiveness (Melghit et al. 2005). Improvement of dielectric materials for applications in communication systems such as substrates, cellular phone, etc. has been rapidly progressing in the past few years (Wolfram and Gobel 1981). Changes in dielectric and optical properties have been associated to changes in size, shape, and particle environment (Veena Gopalan et al. 2008; Shenoy et al. 2004). The tailored dielectric and optical properties were used as capacitors, electronic memories, and optical filters (Subramanian et al. 2000; Ramirez et al. 2000; Jha et al. 2004). The high dielectric permittivity and the low loss factors over a wide frequency range are always of a great interest (Prasad et al. 2011). The dielectric properties of materials are mainly due to contributions from electronic, ionic, dipolar and space charge polarizations. Dipolar or orientation polarization arises from molecules having a permanent electric dipole moment that can change its orientation when an electric field is applied. Space charge polarization arises from molecules having a permanent electric dipole moment that can change its orientation when an electric field is applied. It is established that coupling of different semiconductor metal oxides in the same nanocomposite structure can reduce the electron-hole pair combination under irradiation and consequently, higher photocatalytic activity is achieved. The mixed metal oxide nanocomposite materials with having two different energy-level systems can play an important role in increasing charge separation. Now-a-days, SnO_2 has been exploited as promising photocatalytic material for environmental cleanup (Zhuang et al. 2014). However, the CdO or CdO-based semiconductor heterostructure is to be investigated as photocatalyst, since they have the potential for the visible light photocatalytic application (Kumar et al. 2014; Navarro et al. 2008; Saravanan et al. 2015). Hence, it is anticipated that the combination of CdO and SnO_2 will exhibit new interesting properties and will also be expected to enhance the absorption of visible light. Thus, both CdO and SnO_2 have interesting properties and potential ability in numerous applications and, hence, by coupling them it is possible to exchange their peculiar properties and the CdO- SnO_2 nanocomposite might possess enhanced physical properties which can make it of technological importance. Also,

the recent research result shows that the coating agent like polyvinylpyrrolidone (PVP) was used in the fabrication of nanocomposite to make easy dispersion of composites. The coating agent takes part in an essential function to control the particle size and also to reduce the particle agglomeration in nanoparticles, which makes its extension of usage to various technological applications (Al-Hada et al. 2016; Ahmada et al. 2017). Among the multiple surfactants such as polyvinyl alcohol and polyaniline, the PVP can act as an excellent surface stabilizer in nanoparticles and better reducing agent due to its amphiphilic nature.

Accurate knowledge of optical properties such as complex dielectric function $\varepsilon = \varepsilon_1 + i\varepsilon_2$ and refractive index $\tilde{n} = n + i\kappa$ over a wide photon energy range is important due to their significant influence on all relevant optical applications (Law et al. 2008). For TCO applications in photovoltaic (PV) devices, as an example, the extinction coefficient κ is needed to determine the amount of light passing through the TCO layers down to the absorber layer, and the refractive index n is a design parameter for minimizing surface reflection by generating destructive interference. On the other hand, the ε is directly related to the electronic energy band structure of material and may be completely different at various structural phases, even for the same atom component materials. In previous studies (Freeouf 1973; Altwein et al. 1968; Koffyberg 1976; Mazumder et al. 2020) the ε spectra for CdO and SnO₂ have been calculated from Kramers–Kronig (KK) transformation of the reflectivity data. Spectroscopic ellipsometry (SE) has been utilized as research approach with high accuracy to determine both real and imaginary parts of ε simultaneously without need of the KK transformation. In addition, SE also possesses several advantages over conventional reflectivity techniques in terms of accuracy of the data (Aspnes 1985).

The success of nanocomposites comes from the possibility of obtaining diverse properties depending on the characteristics of their different constituents. The effective characteristic of nanocomposite material depends not only on the physical properties of its constituents, but is also determined by the geometry of such a heterogeneous system. Such as the shape of inclusions, their distribution in the matrix, their orientation according to external constraints, and their volume fraction (concentration). For this, the effective characteristic of nanocomposite material is very complex function, and difficult to describe. To design new material, an analysis of their behavior is required. The possibility of processing such a heterostructure using effective parameters, as well as the influence of inhomogeneities on the behavior of the electric field, is essential in desired applications. The effective permittivity describing the relationships between the microscopic and macroscopic properties of composites, has been described by many analytical and theoretical methods, called effective medium theory (EMT) these are the famous formulas of Clausius Mossotti (CM), Maxwell–Garnett (MG) and Rayleigh (Maxwell–Garnett 1850;1904; Clausius 1879). However, work on EMT is still ongoing, as evidenced by the abundance of bibliography devoted to this topic. The reason for this evolution is that the EMT can only predict the electrical properties of certain particular composite media. The main problems which still arise concern the high inclusions concentrations, inclusions geometry and their distribution. Due to the considerable progress made in modelling and electromagnetic calculations, the efforts and attempts using numerical methods to calculate the effective dielectric permittivity of composites, allowed to get values closer than those given by the analytical EMT. The modeling of composite materials allows their analyzes in a universal way and a saving of time and cost, which is of immense importance for scientific research and industry. Numerical techniques are designed to solve the relevant field equation in the computational domain, subject to the boundary constraints imposed by the geometry. Without making a priori assumption about which the field interactions are most significant, the numerical techniques analyze the entire geometry provided as input. Finite element method (FEM)

(Reddy 1993; Zienkiewicz and Taylor 1989) that is a powerful numerical tool has been widely used for modeling the electromagnetic wave interaction with complex materials. In the present work, density functional theory (DFT) calculation used to calculate the electronic and optical properties of CdO and SnO₂/CdO. After that, the FEM was applied to obtain the optical constants of three TCO nanostructures such as CdO, core/shell SnO₂/CdO and SnO₂/CdO/PVP nanoparticles, the effect of several morphological parameters on the absorption spectrum and optical constants in the ultraviolet–visible–near infrared (UV–Vis–NIR) band are calculated and compared.

The remaining presentation proceeds as follows: We describe, in Sect. 2, the used numerical methodology and computational aspects, in this section we also summarize the calculations formulas of the optical properties like effective permittivity, absorption cross-section, optical complex conductivity and reflectivity for the TCO nanoparticles. Discussion of results is the aim of Sect. 3. Finally, some concluding remarks are drawn in the last section.

2 Computational methods

2.1 First principle calculations

In this work we will use the first principle calculations based on DFT approach and carried out in the Wien2k software (Bickelhaupt and Baerends 2000; Blaha et al. 2001). The calculation of electronic, dielectric and optical properties using DFT calculation, requires determining certain parameters and approximations in input (Kadim et al. 2020, 2021a, b, c; Essalah et al. 2020) such as; The lattice parameters of CdO compound are $a=b=c=3.383$ (Å) and $\alpha=\beta=\gamma=90^\circ$ with the space group Fm3m and of CdSnO₃ are $a=5.554$ (Å), $b=5.678$ (Å), $c=8.036$ (Å) and $\alpha=\beta=\gamma=90^\circ$ with the space group Pnma such as given in Fig. 1. The exchange and correlation energy corrections

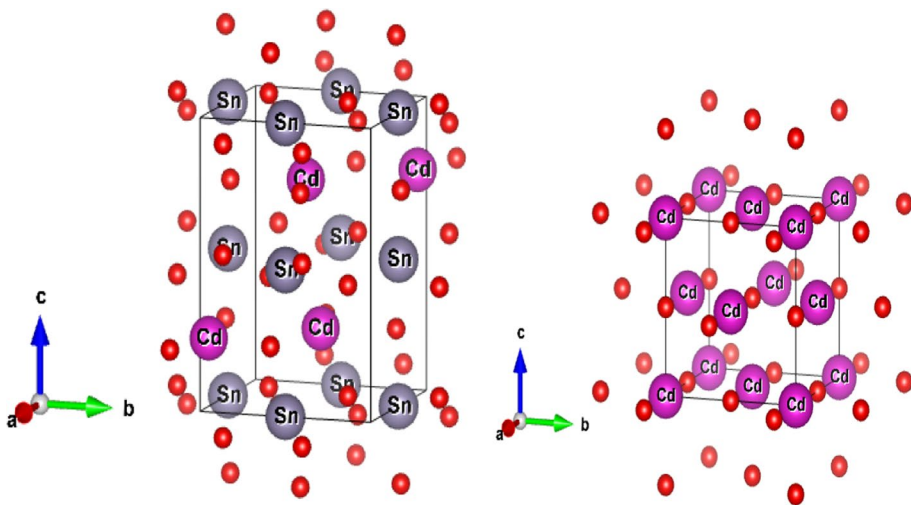


Fig. 1 Structure of CdO (right structure) and CdSnO₃ (left structure) compounds with the red sphere is that of the oxygen atom

included by a generalized gradient approximation (PBE-GGA) and (TB-mBJ); the separation energy between the valence and core states is -9.0 Ry. 1000 k points are used in the full Brillouin zone. The valence wave functions inside the muffin-tin spheres are developed in terms of spherical harmonics up to $l_{\max} = 10$. The $R_{\min}^{MT} k_{\max} = 7.0$, while the charge density was Fourier expanded $G_{\max} = 12$.

2.2 Finite element method

The linear response of a material to an electromagnetic wave is described by dielectric function, which regulates exclusively the proliferation behavior of the radiation within the material. The optical properties of any material can be obtained mainly from dielectric function, as a function of frequency, $\epsilon(\omega) = \epsilon'(\omega) + i\epsilon''(\omega)$ where $\epsilon'(\omega)$ and $\epsilon''(\omega)$ are real and imaginary components of the dielectric function. These last are associated with the inter-band transitions for semiconductor materials, whereas the intra-band transitions are considered only for metallic materials.

Over the past decades, computer simulation has proved itself to be a valuable tool, offering insights into the relationship between the dielectric properties of multiphase composites and their microstructure, an issue of central importance in condensed-matter research due to the wide variety of heterostructures which exist in practice. The optical response of transparent conductive oxide (TCO) nanoparticle is quantified by its complex dielectric constant. The latter is a function of frequency of the electromagnetic wave with which it interacts. Indeed, the interaction of an electromagnetic wave with a pulse, ω , with a TCO nanoparticle will lead to a polarization of the medium. This polarization will then generate a change in the complex refractive index, $\tilde{n}(\omega) = n(\omega) + ik(\omega)$, which is related to the dielectric constant by the relation: $\tilde{n}^2(\omega) = \epsilon(\omega)$. In the nanometric scale, the electronic properties appear when their size is smaller than the mean free path of electrons. From a classical point of view, this corresponds to the fact that the electron surface collisions are not negligible compared to other interaction processes (electron–electron, electron–phonon) and must be taken into account in the rate of the optical collision of electrons.

To investigate in some detail the dielectric properties of heterostructures such as CdO, SnO₂/CdO and PVP coated SnO₂/CdO nanoparticles in the quasistatic limit, a method suitable for determining the effective permittivity is needed. Especially in the case where the inclusions are randomly dispersed in the matrix, FEM is used for the determination of the effective permittivity, a detailed description of the method can be found in literature (Sareni et al. 1996; Myroshnychenko and Brosseau 2005a,b). The aim of this work is to determine the dielectric and optical parameters of multiphase nanoparticles CdO, SnO₂/CdO and PVP Coated SnO₂/CdO which are immersed in dielectric matrix. For this we consider a parallel plate capacitor, with conducting plates of area S and separation distance L which is filled with the composite medium to be studied. The macroscopically inhomogeneous medium consists of different types of materials each of them is characterized by their dielectric permittivity noted ϵ that is a relative quantity compared to the free space permittivity $\epsilon_0 = 8.85310^{-12} \text{ F m}^{-1}$. A constant potential difference ($V_2 - V_1$) is kept between the capacitor plates. Assuming that L is small enough so that fringing effects can be ignored, then the effective permittivity ϵ_{eff} of the composite can be determined from the energy stored in the capacitor. Solving the problem at hand means finding the local potential distribution inside the unit cell volume by solving the first principle of electrostatics, namely the Laplace's Eq. (1):

$$\vec{\nabla} \left(\varepsilon_0 \varepsilon(\vec{r}) \vec{\nabla} V(\vec{r}) \right) = 0, \tag{1}$$

where $\varepsilon(\vec{r})$ and $V(\vec{r})$ are the local relative permittivity and the potential distribution inside the material domain respectively. The implementation of the FEM consists in dividing the three-dimensional domain into tetrahedral finite elements and interpolating the potential V and its normal derivative $\frac{\partial V}{\partial n}$ on each finite element similarly to the BIE method (Sareni et al. 1996; Jebbor and Bri 2012) with the corresponding nodal values.

Having computed the potential and its normal derivative on each tetrahedron of the computational mesh, the electrostatic energy W_e^k , and losses, P_e^k could be expressed for each tetrahedral element as:

$$W_e^k = \frac{\varepsilon_0}{2} \iiint_{V_k} \varepsilon'_k(x, y, z) \left[\left(\frac{\partial V}{\partial x} \right)^2 + \left(\frac{\partial V}{\partial y} \right)^2 + \left(\frac{\partial V}{\partial z} \right)^2 \right] dV_k, \tag{2}$$

$$P_e^k = \frac{\varepsilon_0}{2} \iiint_{V_k} \omega \varepsilon''_k(x, y, z) \left[\left(\frac{\partial V}{\partial x} \right)^2 + \left(\frac{\partial V}{\partial y} \right)^2 + \left(\frac{\partial V}{\partial z} \right)^2 \right] dV_k. \tag{3}$$

where $\varepsilon_k = \varepsilon'_k + i\varepsilon''_k$ and V_k represent the permittivity and the volume of the k th tetrahedron element, respectively. Thus, the total energy W_e and losses P_e in the entire composite can be written by summation over the n_k elements. Then, from the capacitor electrostatic energy expression, we deduce the effective (complex) permittivity $\varepsilon_{eff}(\omega) = \varepsilon'_{eff}(\omega) + i\varepsilon''_{eff}(\omega)$. We find that the real part ε'_{eff} , and imaginary one ε''_{eff} , parallel to the applied electric field, are given by the relationships (4) and (5):

$$\varepsilon'_{eff}(\omega) = W_e \frac{2L}{S(V_2 - V_1)^2} \tag{4}$$

$$\varepsilon''_{eff}(\omega) = P_e \frac{2L}{S\omega(V_2 - V_1)^2} \tag{5}$$

From the evolution of the complex dielectric function depending on the wavelength λ (or frequency ω) of the incident field, The other optical effectives constants such as the refractive index $n(\omega)$, extinction coefficient $\kappa(\omega)$, optical reflectivity $R(\omega)$, absorption cross-sections $\sigma_{abs}(\omega)$ and the complex optical conductivity $\sigma(\omega)$ can be computed through the following relations (Shen 1992; Liu et al. 2014, 2010):

$$n_{eff}(\omega) = \left[\frac{\sqrt{\varepsilon'_{eff}(\omega)^2 + \varepsilon''_{eff}(\omega)^2} + \varepsilon'_{eff}(\omega)}{2} \right]^{1/2} \tag{6}$$

$$\kappa_{eff}(\omega) = \left[\frac{\sqrt{\varepsilon'_{eff}(\omega)^2 + \varepsilon''_{eff}(\omega)^2} - \varepsilon'_{eff}(\omega)}{2} \right]^{1/2} \tag{7}$$

$$R(\omega) = \left| \frac{\sqrt{\epsilon_{eff}(\omega)} - 1}{\sqrt{\epsilon_{eff}(\omega)} + 1} \right|^2 \tag{8}$$

$$\sigma_{abs} = \frac{V_p}{f} \frac{k}{n_{eff}(\omega)} \epsilon''_{eff}(\omega) \tag{9}$$

$$\sigma(\omega) = \sigma_1(\omega) + i\sigma_2(\omega) = -i \frac{\omega}{4\pi} [\epsilon''_{eff}(\omega) - 1] \tag{10}$$

Here, V_p stands for the common volume of nanoparticles, f is their volume fraction, k is the wave-vector amplitude of the electromagnetic wave.

3 Results and discussion

3.1 Optical properties using finite element method

In this work we determined the optical properties using the FEM of three nanoparticles: the first is a monophasic nanoparticle of cadmium oxide CdO, the second is a biphasic core/shell nanoparticle (SnO₂/CdO) consisting of the tin oxide SnO₂-core and a cadmium oxide CdO-shell, the third is a triphasic nanoparticle (SnO₂/CdO/PVP) consisting of SnO₂-core and a CdO-shell both are coated by a second polymeric-shell of polyvinylpyrrolidone PVP. These three nanostructures are periodically distributed in a dielectric matrix characterized by its dielectric permittivity ϵ_m . Two important approaches that intervene in implementation of FEM: the first is the quasistatic approximation, for which the inclusions have small sizes compared to incident electromagnetic wavelength, that's the reason to can consider uniform electric field in the particle. The second is the volume fraction of inclusion relative to the surrounding medium that must be very small to can neglect the interparticle coupling effect.

In a recent work Senthil et al. (2020) showed that the incorporation of SnO₂ and PVP with CdO produces momentous changes in the shape, size and properties. These authors shows that there is a reduction in particle size when SnO₂ and PVP incorporated with CdO and confirms that the nanocomposite contains both a cubical structure of CdO and an orthorhombic structure of SnO₂ and the changes in morphology as nanorod in SnO₂/CdO/PVP due to heterogeneous nucleation effect. In this work we have chosen to model the studied nanoparticles by following geometric shapes: cubic for CdO nanoparticles, orthorhombic core/shell for SnO₂/CdO and nanorod for SnO₂/CdO/PVP. The optical properties of these nanocomposites are studied in the UV–Vis–NIR wavelength band from 190 to 1240 nm. To reach our simulation, the different phases of each considered nanocomposite is characterized by their dielectric permittivity which depends on the frequency of the incident electromagnetic wave, the numerical data of the dielectric constant are taken from the following references: (Choi et al. 2010) for CdO, (Mazumder et al. 2020) for SnO₂ and (König et al. 2014) for PVP.

3.1.1 CdO nanoparticles

Considers a cubic-shaped CdO nanoparticle with edges $a = 20$ nm included in a dielectric medium with a volume fraction $f = 0.1$ defined by relation $f = \frac{V_p}{V_{cel}}$, V_p is the volume of the particle and V_{cel} is that of the simulation cell, the dielectric permittivity of the different constituent denoted by: ϵ_{CdO} for the CdO nanoparticle and ϵ_m for the medium. Figure 2a–h shows the calculated effective values of the complex dielectric function, absorption cross section, optical reflectivity and complex conductivity for different values of the surrounding medium permittivity ϵ_m . Figure 2a and b shows the variation of real and imaginary parts of dielectric constant with the wavelength, respectively. As seen in Fig. 2a, the variation of the real part of dielectric constant is slightly variable around an average value in the UV–Vis–NIR band. As shown in Fig. 2c this average value increases linearly with the surrounding medium permittivity ϵ_m according to the function $\epsilon'_{eff} = 0.4 + 0.92\epsilon_m$, this suggests that the real part of the CdO nanoparticle can be both reduced and increased with the surrounding medium. As seen in Fig. 2b, the imaginary part ϵ''_{eff} of dielectric constant takes a peak in the UV region at $\lambda = 210$ nm, then it decreases with increasing wavelength up to $\lambda = 530$ nm so as to plan at a very low value, these curves also shows that the imaginary part ϵ''_{eff} increases with increases ϵ_m in the (190–530 nm) range and beyond this value ϵ''_{eff} is the same whatever the value of ϵ_m .

The absorption cross section $\sigma_{abs}(\lambda)$ is an important parameter for optical property analysis, it indicates a measure in the intensity of electromagnetic radiation as it passes through any material. $\sigma_{abs}(\lambda)$ is related to the absorption coefficient $\alpha(\lambda)$ and the quantity of absorbent particles N per unit of volume by the relation $\alpha(\lambda) = N\sigma_{abs}(\lambda)$. As light penetrates through any material its intensity gets decreased, the absorption coefficient gives the measure of how much distance a beam of definite energy can penetrate into the material before it being absorbed. The spectral distribution of the absorption cross section is shown in Fig. 2d, the absorbance is high at the hard ultraviolet region and takes a maximum at $\lambda = 210$ nm, the steepest increase of absorption spectra defines the optical bandgap. It was observed from Fig. 2d, the absorption cross section decreases with wavelength increases who becomes negligible above the $\lambda = 530$ nm. Low absorption of the CdO nanoparticles in the visible-IR region makes them suitable for optical fiber and electron transport layer applications. The absorption spectra also show that the $\sigma_{abs}(\lambda)$ increases when the permittivity of the surrounding medium increases from $\epsilon_m = 1$ to $\epsilon_m = 6$ and keeps the same trend when ϵ_m is greater to $\epsilon_m = 6$. The optical conductivity is one of the parameters used to study the optical response of the samples, it is defined as $\sigma(\lambda) = \sigma_1(\lambda) + i\sigma_2(\lambda)$ where $\sigma_1(\lambda)$ is the real part of conductivity and $\sigma_2(\lambda)$ is the imaginary part of conductivity. If a photon with energy greater than the band gap, gets absorbed in a crystal, bound electron–hole pair is generated. These pairs are free to move in the crystal, movement of these bound pair electrons cause the presence of optical conductivity. Optical conductivity is used for designing of optical detectors. Due to electronic charge neutrality, these do not contribute to the electrical conductivity (Dash et al. 2004). Electrical conductivity is negligible for insulators or semiconductors but optical conductivity is always finite after the optical bandgap. The variations of real part of the optical conductivity with wavelength of CdO nanostructures is shown in Fig. 2e. From the figure $\sigma_1(\lambda)$ follows a similar trend as the absorption cross section and imaginary part of permittivity. The variations of imaginary part of optical conductivity with wavelength of CdO nanostructures is shown in Fig. 2f. From the figure $\sigma_2(\lambda)$ takes a minimum value in the UV region, then it gradually increases until it takes a limit value close to zero in the Vis–NIR band. The two Fig. 2e and f show

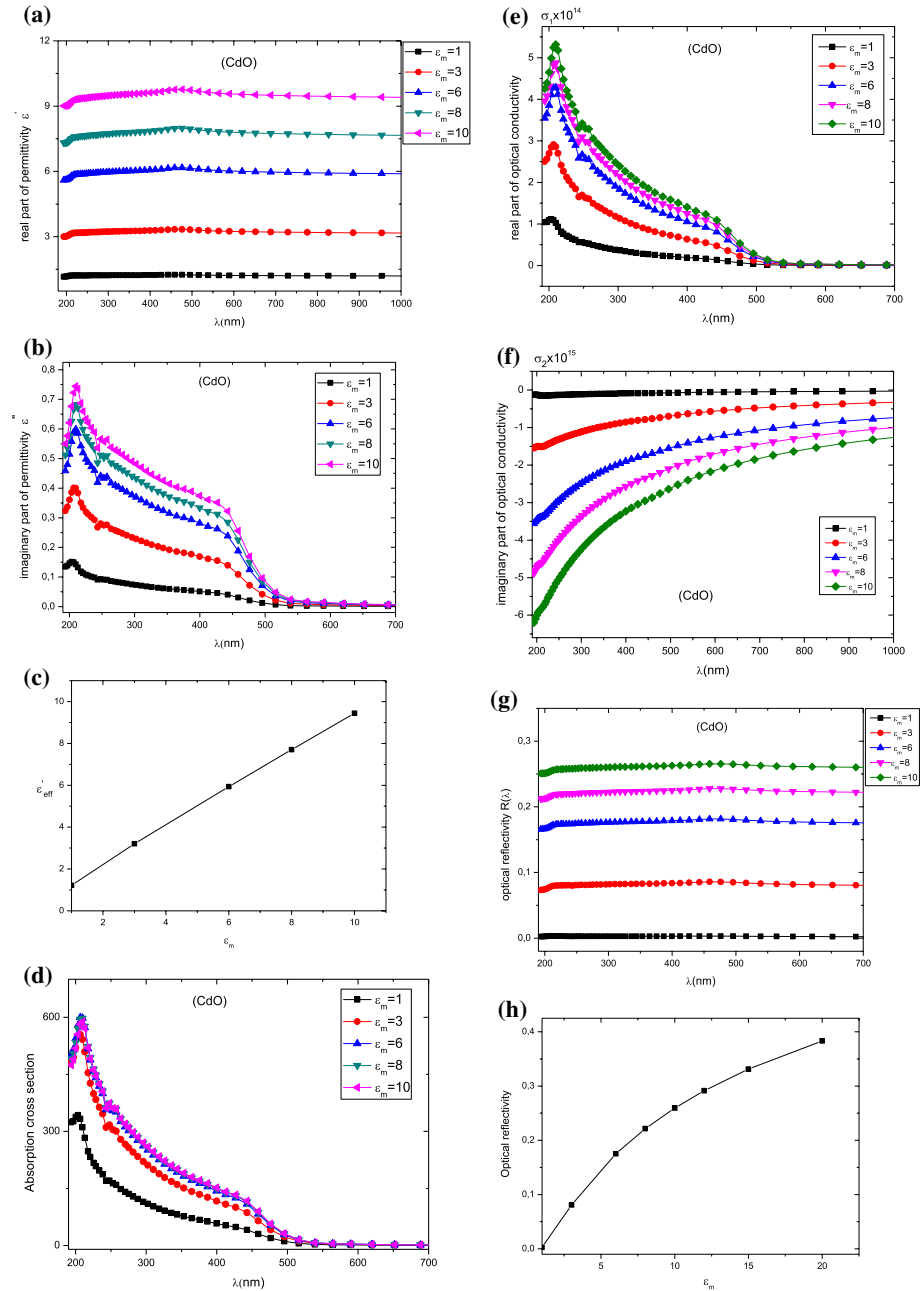


Fig. 2 The spectra of dielectric function (a) real part, (b) imaginary part of CdO nanoparticle for different values of ϵ_m . The chosen parameters are: $a = 20$ nm and $f = 0.1$ nm. (c) The average value of the real part of ϵ_{eff} for CdO nanoparticle with the surrounding medium permittivity ϵ_m . (d) The Absorption spectra of CdO nanoparticle for different values of ϵ_m . The chosen parameters are: $a = 20$ nm and $f = 0.1$ nm. The real (e) and imaginary (f) parts of the optical conductivity for CdO nanoparticle for different values of ϵ_m . The chosen parameters are: $a = 20$ nm and $f = 0.1$ nm. (g) The reflectivity spectra of CdO nanoparticle for different values of ϵ_m . The chosen parameters are: $a = 20$ nm and $f = 0.1$ nm. (h) The average value of reflectivity for CdO nanoparticle with the surrounding medium permittivity ϵ_m

that the real part $\sigma_1(\lambda)$ and the absolute value of $|\sigma_2(\lambda)|$ increase when the permittivity of the surrounding medium increases in all UV–Vis–NIR band. To have further insight into the optical properties of the materials, reflectivity is an important quantity that signifies the amount of light reflected from the material. In Fig. 2g, we have plotted the variation of the reflectivity of CdO nanoparticle with wavelength for different values of surrounding medium permittivity ϵ_m . All plots presented in Fig. 2g show low variation of reflectivity around an average value R_m in the UV–Vis–NIR band, this average value increases when ϵ_m increases. As shown in Fig. 2h the estimated average value R_m can be determined by following relation $R_m(\epsilon_m) = R_0 + Ae^{a\epsilon_m}$ such as, $R_0 = 0.46$, $A = -0.5$ and $\alpha = -0.091$. Which allows to adjust the reflectivity of the CdO nanostructure by modification of surrounding environment. The optical properties of CdO nanoparticles don't just depend on the nature of surrounding environment in which they are immersed, but also on their concentration. Figure 3a–f show the variations of different optical parameters with wavelength for different values of volume fraction f of CdO nanoparticles. For these curves we have fixed the following parameters: size of cubic CdO nanoparticle $a = 20$ nm and permittivity of medium $\epsilon_m = 1$ (air). Figure 3a shows that for low values of volume fraction the real part ϵ'_{eff} varies slightly throughout the UV–Vis–NIR band, then for high volume fraction the real part increases and its spectrum takes a peak around $\lambda = 460$ nm, for $\lambda \geq 700$ nm the real permittivity remains constant whatever the volume fraction. Figure 3b shows the variation of the imaginary part ϵ''_{eff} for different values of the volume fraction f , these curves show that the spectrum of ϵ''_{eff} takes a peak in the UV region in the vicinity of $\lambda = 210$ nm, then it decreases with a shoulder for $\lambda = 460$ nm and remains constant starting from the $\lambda = 530$ nm. We also see, when the volume fraction f increases ϵ''_{eff} increases and the peak becomes more dominant while all curves tighten on the same starting from $\lambda = 530$ nm. Figure 3c shows that the evolution of the real part of optical conductivity $\sigma_1(\lambda)$ with the wavelength is the same as that of ϵ''_{eff} , and when the volume fraction increases $\sigma_1(\lambda)$ also increases. Figure 3d shows the variation of imaginary part of optical conductivity $\sigma_2(\lambda)$ with the wavelength, the obtained spectrum shows that $\sigma_2(\lambda)$ takes a minimum value in the UV band at $\lambda = 210$ nm, then gradually increases in the visible band and remains constant in the NIR region. We also notice that when the volume fraction f increases the minimum value of $\sigma_2(\lambda)$ becomes more dominant and their absolute value increases. Figure 3e shows the plotted reflectivity $R(\lambda)$ of the CdO nanostructure immersed in a dielectric matrix which is air here for different values of the volume fraction f . The obtained spectra show that $R(\lambda)$ takes two small peaks, the first in the UV at $\lambda = 210$ nm and the second in the visible at $\lambda = 460$ nm and slightly varies throughout the UV–Vis–NIR band. The obtained results show the low values of reflectivity in the studied band which varies between $R(\lambda) = 1\%$ and $R(\lambda) = 6\%$ when the fraction increases from $f = 0.1$ to $f = 0.5$ which allows to use these nanocomposites in desired applications.

3.1.2 SnO₂/CdO nanoparticles

Let's interest now to study the optical properties of core/shell nanostructures formed by SnO₂-core and CdO-shell, it is well known that the nanoparticles shape changes from cube to orthorhombic when combining the SnO₂ with CdO (Sareni et al. 1996). To model these nanoparticles, we consider an orthorhombic SnO₂/CdO nanoparticle $a \neq b \neq c$, ($a = 12$ nm, $b = 18$ nm, $c = 24$ nm) included in a dielectric medium of permittivity $\epsilon_m = 1$ (air) with the volume fraction $f = 0.1$. We denote this nanocomposite by $x - SnO_2 / (1 - x) - CdO$ with x representing the mass composition of the nanoparticle

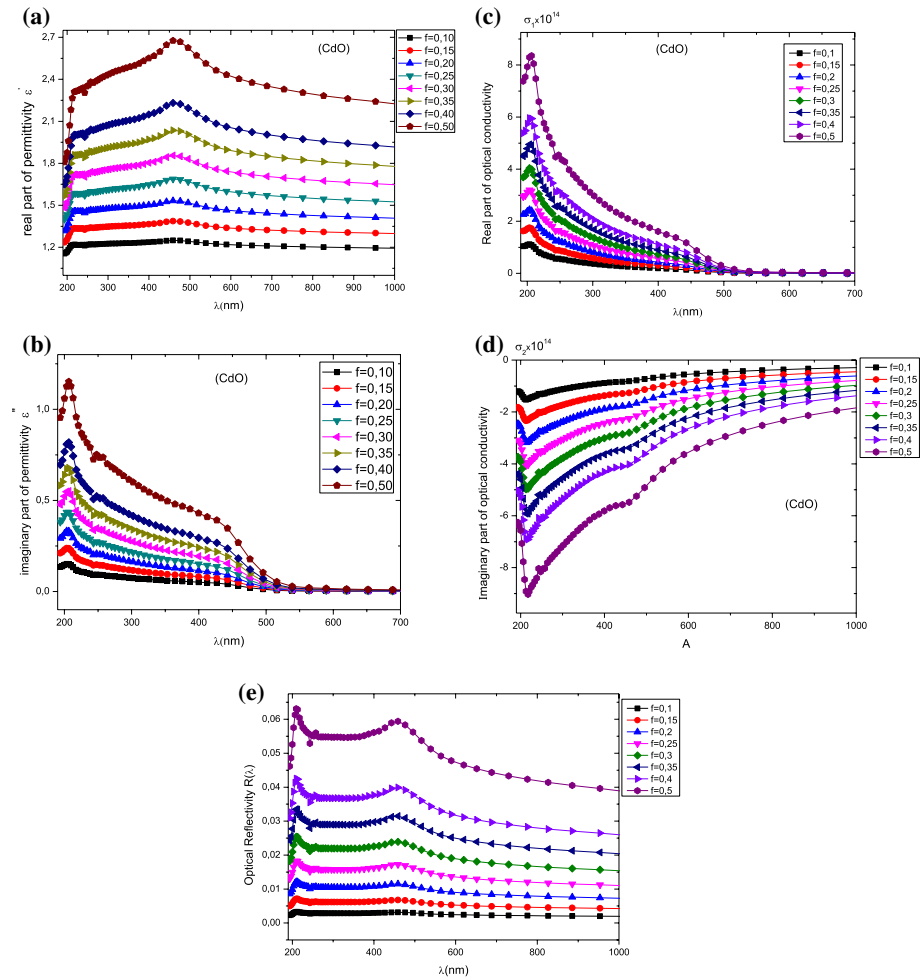


Fig. 3 The spectra of dielectric function **(a)** real part, **(b)** imaginary part of CdO nanoparticle for different values of volume fraction. The chosen parameters are: $a = 20$ nm and $\epsilon_m = 1$. The real **(c)** and imaginary **(d)** parts of the optical conductivity of CdO nanoparticle upon wavelengths for different values of f . The chosen parameters are: $a = 20$ nm and $\epsilon_m = 1$. **(e)** The reflectivity spectra of CdO nanoparticle for different values of f . The chosen parameters are: $a = 20$ nm and $\epsilon_m = 1$

which is defined by $x = \frac{m_{SnO_2}}{m_{SnO_2} + m_{CdO}}$ with m_{CdO} and m_{SnO_2} are respectively the mass quantity of CdO and SnO₂. Figure 4a–f show the calculated optical parameters in the UV–Vis–NIR band with wavelength for different values of the mass composition of CdO and SnO₂. Figure 4a shown spectrum of the real part of dielectric permittivity ϵ'_{eff} for different value of the mass fraction x , in the same figure the spectrum of the single CdO nanoparticle is also represented. These results show that ϵ'_{eff} takes a maximum in the visible band at $\lambda = 460$ nm and when the mass fraction of SnO₂ increases ϵ'_{eff} decreases throughout the UV–Vis–NIR band. Figure 4b shows that the imaginary part of permittivity ϵ''_{eff} has same evolution as that of a single CdO nanoparticle in the UV–Vis–NIR band. These curves show that in the 190–530 nm range when the mass fraction of SnO₂ increases ϵ''_{eff} decreases

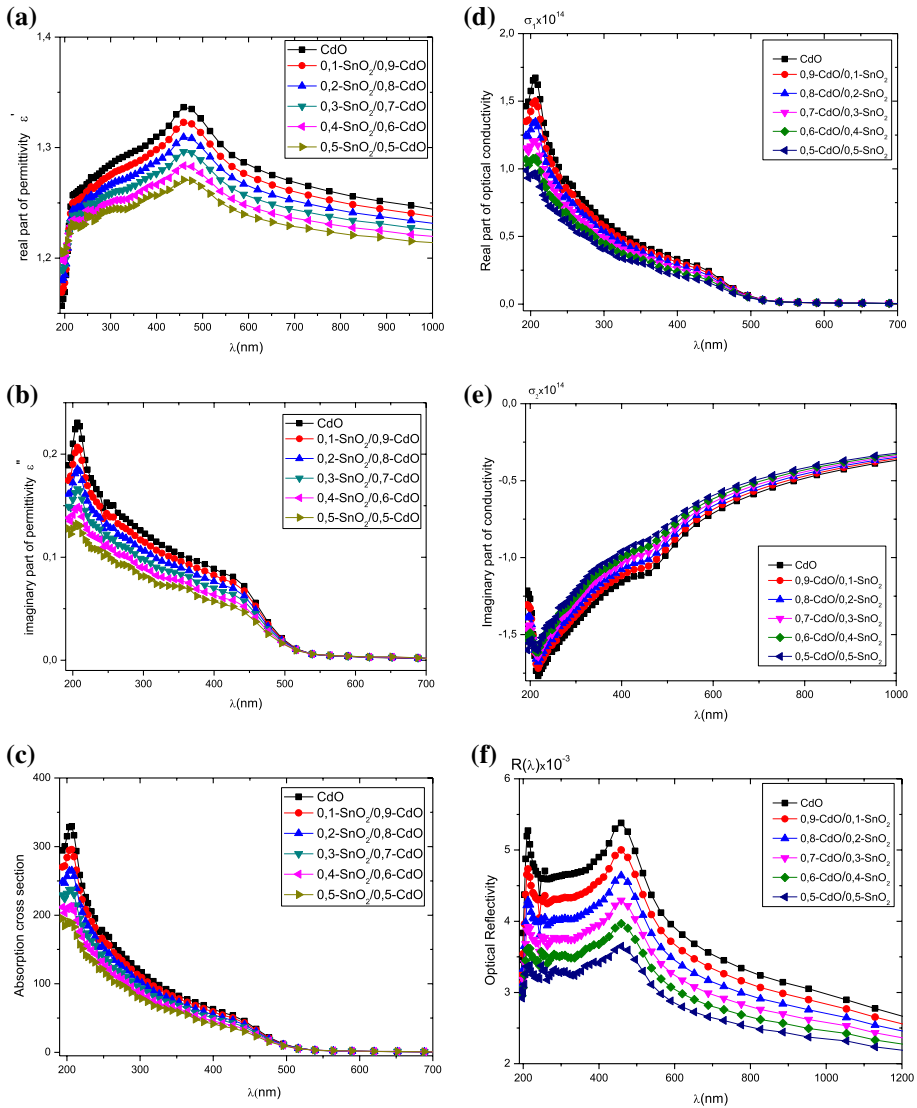


Fig. 4 The spectra of dielectric function (a) real part, (b) imaginary part of $x\text{-SnO}_2/(1-x)\text{-CdO}$ nanoparticle for different values of SnO_2 mass fraction x . **c** The Absorption spectra of $x\text{-SnO}_2/(1-x)\text{-CdO}$ nanoparticle for different values of SnO_2 mass fraction x . The real (d) and imaginary (e) parts of the optical conductivity of $x\text{-SnO}_2/(1-x)\text{-CdO}$ nanoparticle for different values of SnO_2 mass fraction x . **f** The reflectivity spectra of $x\text{-SnO}_2/(1-x)\text{-CdO}$ nanoparticle for different values of SnO_2 mass fraction x

and for $\lambda \geq 530$ nm all the curves fall on that of a single CdO nanoparticle. Figure 4c shows the variation of absorption cross section of $x\text{-SnO}_2/(1-x)\text{-CdO}$ and single CdO nanoparticles with wavelength, as seen in the 190–530 nm range the absorption cross section σ_{abs} decreases when the mass fraction of SnO_2 increases, then in the rest of the Vis–NIR region σ_{abs} does not change in the presence of SnO_2 , these results are in good agreement with that presented in Sirohi et al. (2018). Figure 4d–e show the variation of the

optical complex conductivity for different composition in CdO and SnO₂, we see that the real part $\sigma_1(\lambda)$ takes a peak in the UV region at $\lambda = 210$ nm then decreases up to $\lambda = 530$ nm and becomes zero in the rest of the Vis–NIR band. In the 190–530 nm rang, when the SnO₂ mass fraction increases $\sigma_1(\lambda)$ decreases, and for $\lambda \geq 530$ nm $\sigma_1(\lambda)$ becomes zero whatever the SnO₂ and CdO composition. On the other hand, Fig. 4e shows that the imaginary part $\sigma_2(\lambda)$ increases in the entire UV–Vis–NIR band when the mass fraction of SnO₂ increases, this figure also shows that $\sigma_2(\lambda)$ takes a minimum in the UV region before increasing in the rest of the Vis–NIR band. The reflectivity of the x -SnO₂/(1 - x)-CdO nanoparticle is shown in Fig. 4f, the plotted spectrum of $R(\lambda)$ show the presence of a reflection peak in the visible at $\lambda = 460$ nm, then the reflectivity decreases near the IR region. It is also seen that the reflectivity decreases when the mass fraction of SnO₂ increases. Due to the spatial anisotropy of their orthorhombic structure, the optical behavior of $x - SnO_2/(1 - x) - CdO$ nanoparticle depends on their orientation relative to the incidence direction of the electromagnetic wave. To study the spatial orientation effect of these nanostructures we consider the angle α between the largest axis direction of the particle and that of the electric field. When $\alpha = 0^\circ$ the applied electric field is parallel to longitudinal direction of particle, when $\alpha = 90^\circ$ the electric field is transverse to the particle direction and for $0^\circ < \alpha < 90^\circ$ the particle is inclined compared to the electric field. Figure 5a–f shown the variation of optical parameters with the wavelength for different values of α which varies between 0° and 90° . Figure 5a and f show that the real part of permittivity ϵ'_{eff} and the reflectivity $R(\lambda)$ have the same evolution in the UV–Vis–NIR band, these two quantities take a peak in the visible at $\lambda = 460$ nm and decreased in the entire band where the angle α increases from 0° to 90° . Figure 5b–d show that the imaginary part of the permittivity ϵ''_{eff} , absorption cross section σ_{abs} and the real part of the conductivity $\sigma_1(\lambda)$ have the same evolution in the entire UV–Vis–NIR band. These three quantities take a peak in the UV region at $\lambda = 210$ nm, decrease between $\lambda = 210$ nm and $\lambda = 530$ nm and take a shoulder at $\lambda = 460$ nm, these figures also show that ϵ''_{eff} , σ_{abs} and $\sigma_1(\lambda)$ decrease when the angle α varies from 0° to 90° . Figure 5e shows that the imaginary part of optical conductivity $\sigma_2(\lambda)$ increases when α increases from 0° to 90° and tends to be constant in the NIR region.

3.1.3 SnO₂/CdO/PVP nanoparticles

The third nanostructure that we have studied in this work is a three phasic core/shell nanoparticle, the core is consists by the combination of two oxides SnO₂ and CdO and the shell is the polyvinylpyrrolidone (PVP). In their work Sareni et al. (1996) have shown that the addition of PVP as a coating agent to the SnO₂/CdO nanostructure change the morphology from orthorhombic to rod. In this work, we model this nanostructure by an orthorhombic core-SnO₂/shell-CdO particle coated with a second shell of PVP with nanorod shape. The core composition is chosen as follows: 0.2-SnO₂/0.8-CdO such that 0.2 and 0.8 are the mass fractions of SnO₂and CdO respectively, the size of the SnO₂ internal core is ($a = 12$ nm, $b = 18$ nm, $c = 24$ nm). We use the notation $(1 - y) - (SnO_2/CdO)/y - PVP$ with y is the mass fraction of PVP which is given by the relation $y = \frac{m_{PVP}}{m_p}$, m_{PVP} and m_p are respectively the mass of PVP and particle. Figure 6a–f show the variation of the optical parameters: ϵ'_{eff} , ϵ''_{eff} , σ_{abs} , $\sigma_1(\lambda)$, $\sigma_2(\lambda)$ and $R(\lambda)$ with the wavelength for different values of the outer shell mass fraction (PVP). For these figures, the nanoparticle size changes depending on the PVP mass fraction, the volume fraction is $f = 0.1$ and the surrounding dielectric medium $\epsilon_m = 1$. In these figures we also represent the optical parameters corresponding to monophasic CdO and

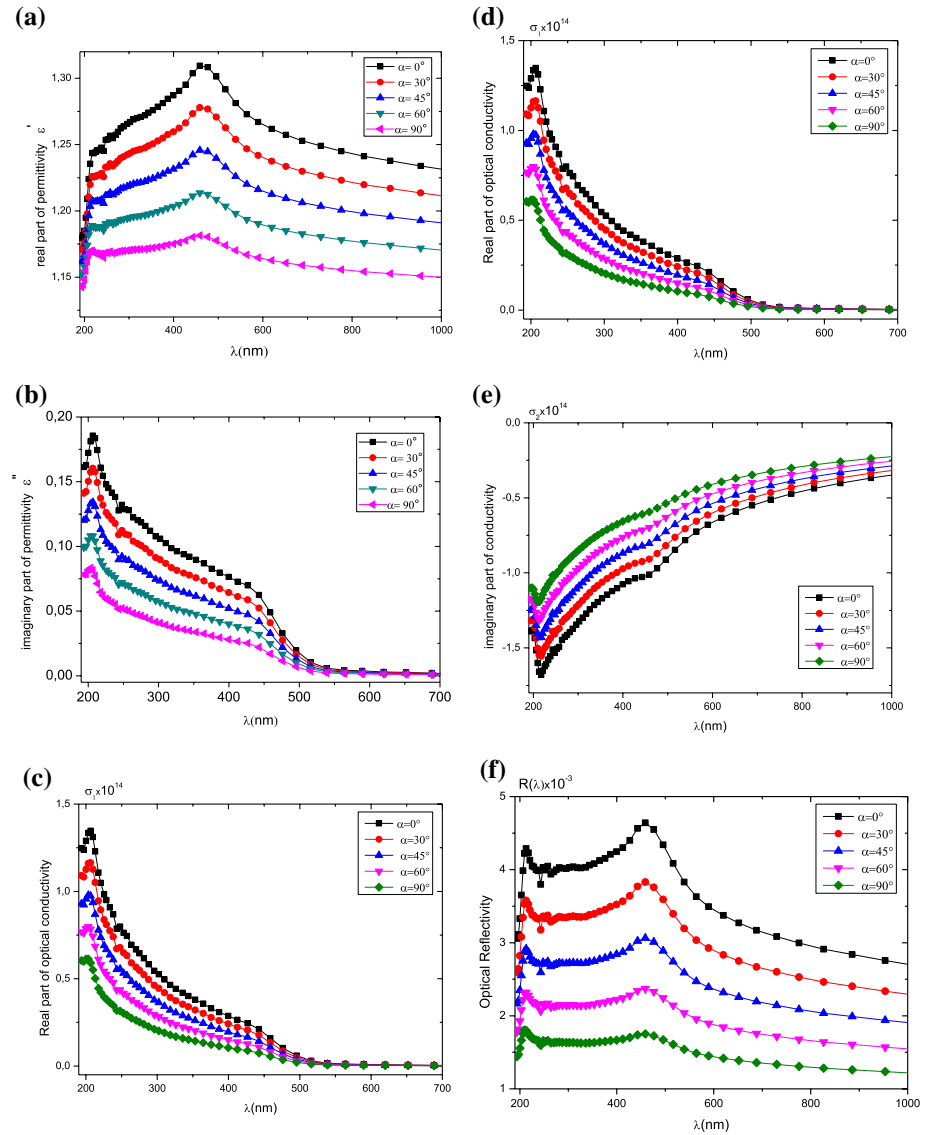


Fig. 5 The spectra of dielectric function (a) real part, (b) imaginary part for $x\text{-SnO}_2/(1-x)\text{-CdO}$ nanoparticle for different values of the angle α . c The Absorption spectra of $x\text{-SnO}_2/(1-x)\text{-CdO}$ nanoparticle for different values of the angle α . The real (d) and imaginary (e) parts of the optical conductivity of $x\text{-SnO}_2/(1-x)\text{-CdO}$ nanoparticle for different values of the angle α . f The reflectivity spectra of $x\text{-SnO}_2/(1-x)\text{-CdO}$ nanoparticle for different values of the angle α

biphasic SnO_2/CdO nanoparticles. These figures show that the spectra of the optical constants ϵ'_{eff} , ϵ''_{eff} , σ_{abs} , $\sigma_1(\lambda)$, $\sigma_2(\lambda)$ and $R(\lambda)$ have the same evolution as those of the CdO and SnO_2/CdO nanostructures in the entire UV–Vis–NIR band with the following changes: A considerable decrease in the constants ϵ'_{eff} , ϵ''_{eff} , $\sigma_1(\lambda)$ and $R(\lambda)$ when introduced the PVP in the SnO_2/CdO structure, this decrease continues by increasing the

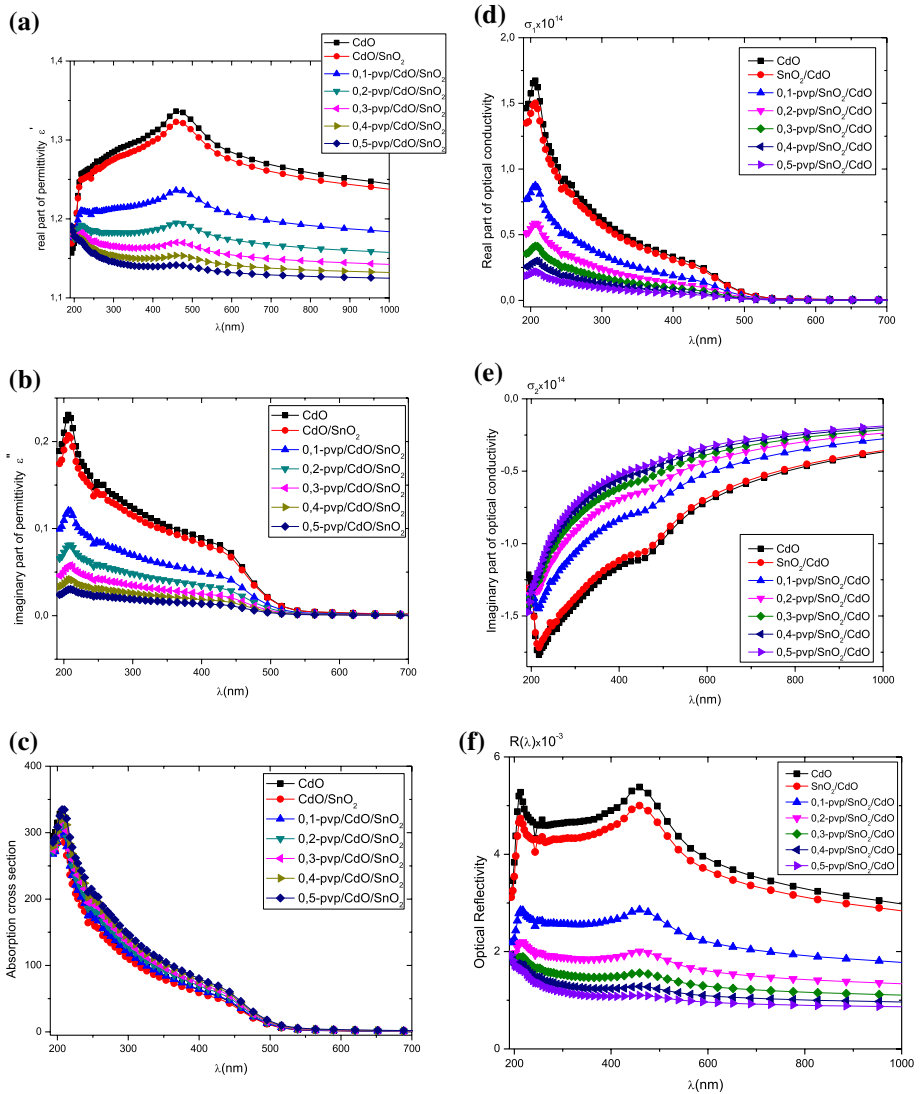


Fig. 6 The spectra of dielectric function (a) real part, (b) imaginary part of $(y - 1)\text{-}(\text{SnO}_2/\text{CdO})/y\text{-PVP}$ nanoparticle for different values of PVP mass fraction y . c The Absorption spectra of $(y - 1)\text{-}(\text{SnO}_2/\text{CdO})/y\text{-PVP}$ nanoparticle for different values of VP mass fraction y . The real (d) and imaginary (e) parts of the optical conductivity of $(y - 1)\text{-}(\text{SnO}_2/\text{CdO})/y\text{-PVP}$ nanoparticle for different values of PVP mass fraction y . f The reflectivity spectra of $(y - 1)\text{-}(\text{SnO}_2/\text{CdO})/y\text{-PVP}$ nanoparticle for different values of PVP mass fraction y

PVP mass fraction. The absorption cross section σ_{abs} decreases in the 190–530 nm rang when SnO_2 is added to CdO and comes back to increase by adding the PVP this increase continues as the PVP mass fraction increases. The imaginary part of the optical conductivity $\sigma_2(\lambda)$ increases slightly when switching from CdO to SnO_2/CdO and increases strongly when adding the PVP.

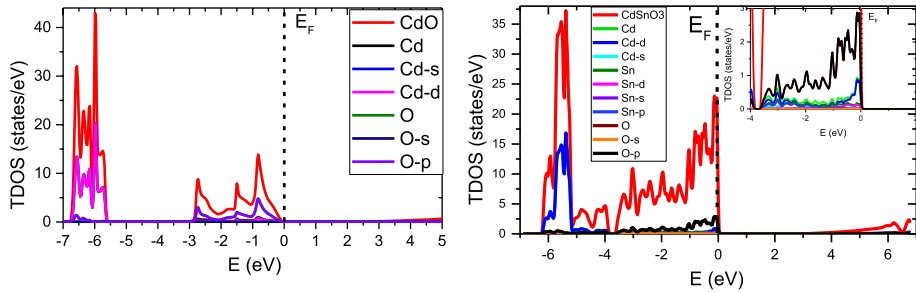


Fig. 7 Total and PDOS (b–d) of CdO and CdSnO₃ compounds calculated using GGA + TB-mBJ approximation

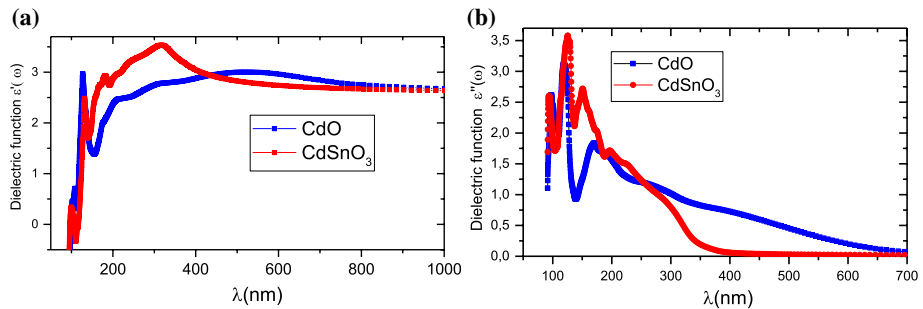


Fig. 8 Variation of Real $\epsilon'(\omega)$ (a) and imaginary $\epsilon''(\omega)$ parts (b) of dielectric $\epsilon(\omega)$ for CdO and CdSnO₃ compounds calculated using GGA + TB-mBJ approximation

3.2 Electronic and optical properties using DFT calculation

The ab-initio approach in real space of electronic structure calculations based on the finite element method, is an approach brings a new quality to the resolution of Kohn Sham's equations, to the calculation of electronic states, of total energy, Hellmann–Feynman forces and material properties, especially for non-crystalline and non-periodic structures (Vackář et al. 2012).

The peaks that appear in optical properties are usually due to the electronic transition. In order to study these peaks, the electronic properties must be calculated and analyzed. The calculated (PDOS and TDOS) densities of states for CdO and CdSnO₃ are displayed in Fig. 7 within the energy interval from -7 to 6 eV. In two compounds CdO and CdSnO₃; there is a large electron contribution of O-p and Cd-d near fermi E_F energy and in the region $[-7$ eV, -5 eV]. This indicates that the hybridization occurs between O-2p and Cd-d (Bououdina et al. 2015). Underline that the gap value closest to Fermi level E_F is due mainly of Cd-d and O-p. The gap values of CdO and CdSnO₃ are 2.75 eV and 3.33 eV respectively. These values are reasonable compared to the experimental value 2.75 eV, 2.36 eV and 3.07 eV (Thomas and Abraham 2015; Tripathi et al. 2016; Natu and Wu 2010).

The calculated $\epsilon(\omega)$ spectra is plotted in Fig. 8a. The negative value of $\epsilon_1(\omega)$ is in the range of beyond 100 nm for CdO and CdSnO₃. This show that in this range most of the electromagnetic wave reflected from the medium and the materials reveal metallic

behavior. The imaginary part $\epsilon''(\omega)$ of complex dielectric function is illustrated in Fig. 8b for CdO and CdSnO₃. The maximum peak appears near 150.66 nm and 171.50 nm for CdO and CdSnO₃ respectively. The absorption edge region is extended from 100 to 805 nm for CdO and from 100 to 400 nm for CdSnO₃. The width of this region depends on the size of the valence and conduction band region. This high peak originates due to the transition of electrons from d-state of Cr and p-state of O in valence band.

The absorption spectrum for CdO and CdSnO₃ are presented in Fig. 9a. In CdO absorption starts at smaller energy compared to the CdSnO₃. This due to the band gap value of CdO compound. Figure 9b display the reflectivity of CdO and CdSnO₃. Its starts at 0.053%. The peaks appear in absorption and reflectivity spectrum is due to the transition of electrons from d-state of Cr and p-state of O in valence band.

4 Conclusion

In summary, the electronic, optical and dielectric properties of CdO, SnO₂/CdO and SnO₂/CdO/PVP nanocomposites were calculated and studied using the numerical finite element and DFT method. The ground states of the compounds have semiconductor character. The peak appear in optical properties is due to the transition of electrons from d-state of Cr and p-state of O in valence band. The high peaks are observed in the small band gap and the peaks height decrease as the band gap increased. In addition, the absorption spectrum increase beyond the gap energy become high in the ultraviolet region. The first structure that we studied in this work is the cubic cadmium oxide CdO nanoparticle, the obtained results show that the optical constants of these nanoparticles depend on their volume fraction and nature of surrounding medium. The spectrum of these parameters takes a peak in the UV, gradually decreases in the visible and cancels out beyond $\lambda = 530$ nm. The spectra of real part of the permittivity and reflectivity are also similar, these two quantities take a maximum value in the visible and vary slightly in the rest of UV–Vis–NIR band. The spectrum of the imaginary part of conductivity shows that the latter takes negative values throughout the UV–Vis–NIR band and takes a peak down in UV region. The optical properties of x -SnO₂/(1 - x)-CdO core/shell nanoparticle is calculated in the UV–Vis–NIR band. The study of the effect of the mass fraction in SnO₂ shows that when x increases, the real and imaginary parts of permittivity, absorption, reflectivity and the real part of conductivity decrease, and the imaginary part of conductivity increases. The optical properties of SnO₂/CdO/PVP nanorods constituted by 0.1 - SnO₂/0.9 - CdO core coated with a PVP shell were studied. The produced calculations show that the optical constants spectra of

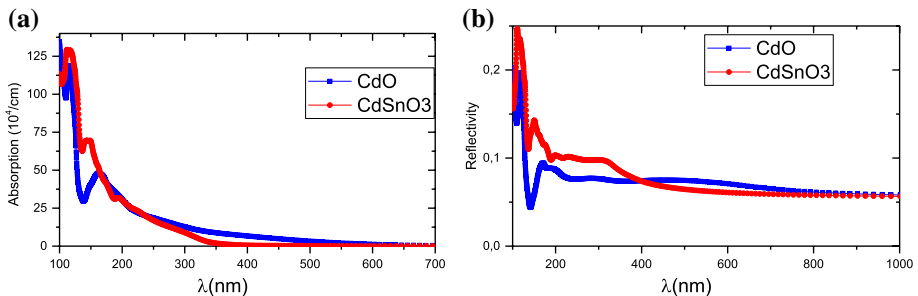


Fig. 9 Variation of absorption (a) and reflectivity (b) for CdO and CdSnO₃ compounds calculated using GGA + TB-mBJ approximation

$\text{SnO}_2/\text{CdO}/\text{PVP}$ nanoparticles have the same evolutions as those of CdO and $\text{SnO}_2/\text{CdO}/\text{PVP}$ nanoparticles. On the basis of suitable semiconductor and good optical properties this material is potential candidates for the photovoltaic applications.

References

- Ahmada, H.A., Saidena, N.M., Saiona, E., Azisa, R.S., Mamat, M.S., Hashim, M.: Effect of PVP as a capping agent in single reaction synthesis of nanocomposite soft/hard ferrite nanoparticles. *J. Magn. Magn. Mater.* **428**, 219–222 (2017). <https://doi.org/10.1016/j.jmmm.2016.12.047>
- Al-Hada, N.M., Saion, E., Kamari, H.M., Flaifel, M.H., Shaari, A.H., Talib, Z.A., Abdullahi, N., Baqer, A.A., Kharazmi, A.: Structural, morphological and optical behaviour of PVP capped binary $(\text{ZnO})-0.4(\text{CdO})-0.6$ nanoparticles synthesised by a facile thermal route. *Mater. Sci. Semicond. Process.* **53**, 56–65 (2016). <https://doi.org/10.1016/j.mssp.2016.06.004>
- Altwein, M., Finkenrath, H., Konak, C., Stuke, J., Zimmerer, G.: The electronic structure of CdO II. Spectral distribution of optical constants. *Phys. Status Solidi* **29**, 203–209 (1968). <https://doi.org/10.1002/pssb.19680290123>
- Anitha, V.S., Sujatha Lakshmy, S., Joy, K.: Effect of Mn doping on the structural, magnetic, optical and electrical properties of $\text{ZrO}_2\text{-SnO}_2$ thin films prepared by sol–gel method. *J. Alloys Compd.* **675**, 331–340 (2016). <https://doi.org/10.1016/j.jallcom.2016.03.045>
- Aspnes, D.E.: The Accurate Determination of optical properties by ellipsometry. In: Palik, E.D. (ed.) *Handbook of Optical Constants of Solids*, vol. I, p. 91. Academic, Orlando (1985)
- Bickelhaupt, F.M., Baerends, E.J.: Kohn-Sham density functional theory: predicting and understanding chemistry. *Rev. Comput. Chem.* **15**, 1–86 (2000)
- Blaha, P., Schwarz, K., Madsen, G.K.H., Kvasnicka, D., Luitz, J.: WIEN2k, an Augmented Plane Wave þ Local Orbitals Program for Calculating Crystal Properties, Karlheinz Schwarz. Technical Universitat Wien, Vienna (2001)
- Bououdina, M., Dakhel, A.A., El-Hilo, M., Anjum, D.H., Kanoun, M.B., Goumri-Said, S.: Revealing a room temperature ferromagnetism in cadmium oxide nanoparticles: an experimental and first-principles study. *RSC Adv.* **5**(42), 33233–33238 (2015)
- Chen, X., Shen, S., Guo, L., Mao, S.S.: Semiconductor-based photocatalytic hydrogen generation. *Chem. Rev.* **110**, 6503–6570 (2010). <https://doi.org/10.1021/cr1001645>
- Choi, S.G., Zúñiga-Pérez, J., Muñoz-Sanjosé, V., Norman, A.G., Perkins, C.L., Levi, D.H.: Complex dielectric function and refractive index spectra of epitaxial CdO thin film grown on r-plane sapphire from 0.74 to 6.45 eV. *J. Vac. Sci. Technol. B* **28**, 1120–1124 (2010). <https://doi.org/10.1116/1.3498755>
- Clausius, R.: Die mechanische U'grmtheorie. **2**, 62 (1879)
- Dash, L.K., Vast, N., Baranek, P., Reining, M.C., Cheynet, L.: Electronic structure and electron energy-loss spectroscopy of ZrO_2 zirconia. *Phys. Rev. B* **70**(24), 245116 (2004). <https://doi.org/10.1103/PhysRevB.70.245116>
- Essalah, G., Kadim, G., Jabar, A., Masrour, R., Ellouze, M., Guermazi, H., Guermazi, S.: Structural, optical, photoluminescence properties and Ab initio calculations of new $\text{Zn}_2\text{SiO}_4/\text{ZnO}$ composite for white light emitting diodes. *Ceram. Int.* **46**(8), 12656–12664 (2020)
- Freeouf, J.L.: Far-ultraviolet reflectance of II–VI compounds and correlation with the Penn-Phillips gap. *Phys. Rev. B* **7**, 3810–3830 (1973). <https://doi.org/10.1103/PhysRevB.7.3810>
- Fujishima, A., Honda, K.: Electrochemical photolysis of water at a semiconductor electrode. *Nature* **238**, 37–38 (1972). <https://doi.org/10.1038/238037a0>
- Jebbor, N., Bri, S.: Effective permittivity of periodic materials: numerical modeling by the finite element method. *J. Electrostat.* **70**(4), 393–399 (2012). <https://doi.org/10.1016/j.elstat.2012.05.007>
- Jha, P., Rai, S., Ramanujachary, K.V., Lofland, S.E., Ganguli, A.K.: $\text{La}_{0.4}\text{Ba}_{0.4}\text{Ca}_{0.2}(\text{Mn}_{0.4}\text{Ti}_{0.6})\text{O}_3$: a new titanomanganate with a high dielectric constant and antiferromagnetic interactions. *J. Solid State Chem.* **177**(8), 2881–2888 (2004). <https://doi.org/10.5281/zenodo.1110608>
- Jin, S., Yang, Y., Medvedeva, J.E., Wang, L., Li, S., Cortes, N., Freeman, A.J.: Tuning the properties of transparent oxide conductors. Dopant ion size and electronic structure effects on CdO -based transparent conducting oxides. Ga- and indoped CdO thin films grown by MOCVD. *Chem. Chem. Mater.* **20**, 220–230 (2007). <https://doi.org/10.1021/cm702588m>
- Kadim, G., Masrour, R., Jabar, A.: Large magnetocaloric effect, magnetic and electronic properties in Ho_3Pd_2 compound: Ab initio calculations and Monte Carlo simulations. *J. Magn. Magn. Mater.* **499**, 166263 (2020)

- Kadim, G., Masrour, R., Jabar, A.: Magnetocaloric effect, electronic and magnetic properties of $\text{Ba}_{1-x}\text{Sr}_x\text{FeO}_3$ barium–strontium ferrites: Monte Carlo simulations and comparative study between TB-mBJ and GGA+U. *Mater. Today Commun.* **26**, 102071 (2021a)
- Kadim, G., Masrour, R., Jabar, A.: Ferroelectric, quantum efficiency and photovoltaic properties in perovskite BiFeO_3 thin films: first principle calculations and Monte Carlo study. *Int. J. Energy Res.* **45**, 9961–9969 (2021b)
- Kadim, G., Masrour, R., Jabar, A.: A comparative study between GGA, WC-GGA, TB-mBJ and GGA+U on magnetocaloric effect, electronic, optic and magnetic properties of BaMnS_2 compound: DFT calculation and Monte Carlo simulation. *Phys. Scr.* **96**, 045804 (2021c)
- Karthik, K., Dhanuskodi, S., Gobinath, C., Prabukumar, S., Sivaramakrishnan, S.: Nanostructured CdO–NiO composite for multifunctional applications. *Chem. Solids* **112**, 106–118 (2018a). <https://doi.org/10.1016/j.jpcs.2017.09.016>
- Karthik, K., Dhanuskodi, S., Gobinath, C., Prabukumar, S., Sivaramakrishnan, S.: Multifunctional properties of CdO nanostructures synthesised through microwave assisted hydrothermal method. *Mater. Res. Innov.* **22**, 1–9 (2018b). <https://doi.org/10.1080/14328917.2018.1475443>
- Koffyberg, F.P.: Thermoreflectance spectra of CdO: band gaps and band-population effects. *Phys. Rev. B* **13**, 4470–4476 (1976). <https://doi.org/10.1103/PhysRevB.13.4470>
- König, T.A.F., Ledin, P.A., Kerszulis, J., Mahmoud, M.A., El-Sayed, M.A., Reynolds, J.R., Tsukruk, V.V.: Electrically tunable plasmonic behavior of nanocube-polymer nanomaterials induced by a redox-active electrochromic polymer. *ACS Nano* **8**(6), 6182–6192 (2014). <https://doi.org/10.1021/nn501601e>
- Kumar, P.S., Selvakumar, M., Bhagabati, P., Bharathi, B., Karuthapandian, S., Balakumar, S.: CdO/ZnO nano-hybrids: facile synthesis and morphologically enhanced photocatalytic performance. *RSC Adv.* **4**, 32977–32986 (2014). <https://doi.org/10.1039/C4RA02502D>
- Lan, M., Fan, G., Yang, L., Li, F.: Enhanced visible-light-induced photocatalytic performance of a novel ternary semiconductor coupling system based on hybrid Zn–In mixed metal oxide/ $g\text{-C}_3\text{N}_4$ composites. *RSC Adv.* **5**, 5725–5734 (2015). <https://doi.org/10.1039/C4RA07073A>
- Law, M., Beard, M.C., Choi, S., Luther, J.M., Hanna, M.C., Nozik, A.J.: Determining the internal quantum efficiency of PbSe nanocrystal solar cells with the aid of an optical model. *Nano Lett.* **8**(11), 3904–3910 (2008). <https://doi.org/10.1021/nl802353x>
- Liu, Q.-J., Liu, Z.-T., Feng, L.-P.: First-principles calculations of structural, electronic and optical properties of tetragonal SnO_2 and SnO. *Comput. Mater. Sci.* **47**, 1016–1022 (2010). <https://doi.org/10.1016/j.commat.2009.11.038>
- Liu, Q.-J., Zhang, N.-C., Liu, F.-S., Liu, Z.-T.: Structural, electronic, optical, elastic properties and Born effective charges of monoclinic HfO_2 from first-principles calculations. *Chin. Phys. B* **23**(4), 047101 (2014). <https://doi.org/10.1088/1674-1056/23/4/047101>
- Makori, N.E., Amatalo, I.A., Karimi, P.M., Njoroge, W.K.: Optical and electrical properties of CdO: Sn thin films for solar cell applications. *Int. J. Optoelect. Eng.* **4**, 11–15 (2014). <https://doi.org/10.5923/j.ijoe.20140401.03>
- Manjula, N., Selvan, G., Balu, A.R.: Improved photodegradation activity of SnO_2 nanopowder against methyl orange dye through Ag doping. *J. Mater. Sci. Mater. Electron.* **29**, 3657–3664 (2017). <https://doi.org/10.1007/s10854-017-8296-1>
- Maxwell-Garnett, J.C.: Colours in metal glasses and in metallic films. *Philos. Trans. r. Soc. A* **203**(359–371), 385–420 (1904). <https://doi.org/10.1098/rsta.1904.0024>
- Mazumder, J.T., Mayengbam, R., Tripathy, S.K.: Theoretical investigation on structural, electronic, optical and elastic properties of TiO_2 , SnO_2 , ZrO_2 and HfO_2 using SCAN meta-GGA functional: a DFT study. *Mater. Chem. Phys.* **254**, 123474 (2020). <https://doi.org/10.1016/j.matchemphys.2020.123474>
- Melghit, K., Mohammed, A.K., Al-Amri, I.: Chimie douce preparation, characterization and photocatalytic activity of nanocrystalline SnO_2 . *Mater. Sci. Eng. B* **117**, 302–306 (2005). <https://doi.org/10.1016/j.mseb.2004.12.021>
- Mossotti, O.F.: *Mem. di mathem. e fisica in Modena*. **24**, 49 (1850)
- Myroshnychenko, V., Brosseau, C.: Finite-element modeling method for the prediction of the complex effective permittivity of two-phase random statistically isotropic heterostructures. *J. Appl. Phys.* **97**, 044101 (2005a). <https://doi.org/10.1063/1.1835544>
- Myroshnychenko, V., Brosseau, C.: Finite-element method for calculation of the effective permittivity of random inhomogeneous media. *Phys. Rev. E* **71**, 016701 (2005b). <https://doi.org/10.1103/PhysRevE.71.016701>
- Natu, G., Wu, Y.: Photoelectrochemical study of the ilmenite polymorph of CdSnO_3 and its photoanodic application in dye-sensitized solar cells. *J. Phys. Chem. C* **114**(14), 6802–6807 (2010)
- Navarro, R.M., Valle, F.D., Fierro, J.L.G.: Photocatalytic hydrogen evolution from CdS–ZnO–CdO systems under visible light irradiation: effect of thermal treatment and presence of Pt and Ru cocatalyst. *Int. J. Hydrog. Energy* **33**, 4265–4273 (2008). <https://doi.org/10.1016/j.ijhydene.2008.05.048>

- Prasad, B.V., Narsinga Rao, G., Chen, J.W., Suresh Babu, D.: Abnormal high dielectric constant in SmFeO_3 semiconductor ceramics. *Mater. Res. Bull.* **46**(10), 1670–1673 (2011). <https://doi.org/10.1016/j.materresbull.2011.06.001>
- Rakibuddin, M., Ananthkrishnan, R.: Effective photocatalytic dechlorination of 2,4-dichlorophenol by a novel graphene encapsulated $\text{ZnO}/\text{Co}_3\text{O}_4$ core-shell hybrid under visible light. *Photochem. Photobiol. Sci.* **15**, 86–98 (2016). <https://doi.org/10.1039/C5PP00305A>
- Ramirez, A.P., Subramanian, M.A., Gardel, M.: Giant dielectric constant response in a copper-titanate. *Solid State Commun.* **115**(5), 217–220 (2000). [https://doi.org/10.1016/S0038-1098\(00\)00182-4](https://doi.org/10.1016/S0038-1098(00)00182-4)
- Reddy, J.N.: *An Introduction to Finite Element Method*. McGraw-Hill Inc., New York (1993)
- Reddy, C.V., Babu, B., Shim, J.: Synthesis, optical properties and efficient photocatalytic activity of CdO/ZnO hybrid nanocomposite. *J. Phys. Chem. Solids* **112**, 20–28 (2018). <https://doi.org/10.1016/j.jpcs.2017.09.003>
- Saravanan, R., Khan, M.M., Gupta, V.K., Mosquera, E., Gracia, F., Narayanang, V., Stephen, A.: $\text{ZnO}/\text{Ag}/\text{CdO}$ nanocomposite for visible light induced photocatalytic degradation of industrial textile effluents. *J. Colloid Interface Sci.* **452**, 126–133 (2015). <https://doi.org/10.1016/j.jcis.2015.04.035>
- Sareni, B., Krähenbühl, L., Beroual, A., Brosseau, C.: Effective dielectric constant of periodic composite materials. *J. Appl. Phys.* **80**(3), 1688–1696 (1996). <https://doi.org/10.1063/1.362969>
- Senthil, S., Srinivasan, S., Thangeeswari, T., Madhu, B.J., Silambarasan, M.: Enhanced dielectric, EMI shielding effectiveness, linear and nonlinear optical properties of CdO/SnO_2 nanocomposites. *Nano-Struct. Nano-Objects* **24**, 100554 (2020). <https://doi.org/10.1016/j.nanoso.2020.100554>
- Shen, X.C.: *Semiconductor Spectroscopy and Optical Properties*, 2nd edn., p. 76. Science Press, Beijing (1992). (in Chinese)
- Shenoy, S.D., Joy, P.A., Anantharaman, M.R.: Effect of mechanical milling on the structural, magnetic and dielectric properties of coprecipitated ultrafine zinc ferrite. *J. Magn. Magn. Mater.* **269**(2), 217–226 (2004). [https://doi.org/10.1016/S0304-8853\(03\)00596-1](https://doi.org/10.1016/S0304-8853(03)00596-1)
- Sirohi, K., Kumar, S., Singh, V., Vohra, A.: Synthesis and characterization of $\text{CdO}-\text{SnO}_2$ nanocomposites prepared by hydrothermal method. *Acta Metall. Sin. (Engl. Lett.)* **31**(3), 254–262 (2018). <https://doi.org/10.1007/s40195-017-0659-3>
- Subrahmanyam, A., Ananthkrishnan, R., Rakibuddin, M., Ramesh, T.P., Kiran, M.R., Shankari, D., Chandrasekhar, K.: Efficacy of titanium doped-indium tin oxide ($\text{Ti}/\text{TiO}_2\text{-ITO}$) films in rapid oxygen generation under photocatalysis and their suitability for bio-medical application. *Phys. Chem. Chem. Phys.* **16**, 24790–24799 (2014). <https://doi.org/10.1039/C4CP02819H>
- Subramanian, M.A., Li, D., Duan, N., Reisner, B.A., Sleight, A.W.: High dielectric constant in $\text{ACu}_3\text{Ti}_4\text{O}_{12}$ and $\text{ACu}_3\text{Ti}_3\text{FeO}_{12}$ phases. *J. Solid State Chem.* **151**(2), 323–325 (2000). <https://doi.org/10.1006/jssc.2000.8703>
- Thomas, P., Abraham, K.E.: Excitation wavelength dependent visible photoluminescence of CdO nanomorphotypes. *J. Lumin.* **158**, 422–427 (2015)
- Tripathi, R., Dutta, A., Das, S., Kumar, A., Sinha, T.P.: Dielectric relaxation of CdO nanoparticles. *Appl. Nanosci.* **6**(2), 175–181 (2016)
- Vackář, J., Čertík, O., Cimrman, R., Novák, M., Šipr, O., Plešek, J.: Finite element method in density functional theory electronic structure calculations. In: Hoggan, P., Brändas, E., Maruani, J., Piecuch, P., Delgado-Barrio, G. (eds.) *Advances in the Theory of Quantum Systems in Chemistry and Physics*. Progress of Theoretical and Experimental Physics, vol. 22, pp. 199–217. Dordrecht, Springer (2012). https://doi.org/10.1007/978-94-007-2076-3_12
- Veena Gopalan, E., Malini, K.A., Saravanan, S., Sakthi Kumar, D., Yoshida, Y., Anantharaman, M.R.: Evidence for polaron conduction in nanostructured manganese ferrite. *J. Phys. D Appl. Phys.* **41**, 185005 (2008). <https://doi.org/10.1088/0022-3727/41/18/185005>
- Wolfram, G., Gobel, H.E.: Existence range, structural and dielectric properties of $\text{Zr}_x\text{Ti}_y\text{Sn}_z\text{O}_4$ ceramics ($x + y + z = 2$). *Mater. Res. Bull.* **16**, 1455–1463 (1981). [https://doi.org/10.1016/0025-5408\(81\)90066-0](https://doi.org/10.1016/0025-5408(81)90066-0)
- Zhao, Z., Morel, D.L., Ferekides, C.S.: Electrical and optical properties of tin-doped CdO films deposited by atmospheric metalorganic chemical vapor deposition. *Thin Solid Films* **413**, 203–211 (2002). [https://doi.org/10.1016/S0040-6090\(02\)00344-9](https://doi.org/10.1016/S0040-6090(02)00344-9)
- Zhuang, S., Xu, X., Feng, B., Hu, J., Pang, Y., Zhou, G., Tong, L., Zhou, Y.: Photogenerated carriers transfer in dye-graphene- SnO_2 composites for highly efficient visible-light photocatalysis. *ACS Appl. Mater. Interfaces* **6**, 613–621 (2014). <https://doi.org/10.1021/am4047014>
- Zienkiewicz, O.C., Taylor, R.L.: *The Finite Element Method*, vol. 1. McGraw-Hill, London (1989)